Bull. Chem. Soc. Ethiop. **2027**, 41(1), 15-27.
DOI: https://dx.doi.org/10.4314/bcse.v41i1.2

ISSN 1011-3924
Printed in Ethiopia
Online ISSN 1726-801X
© 2027 Chemical Society of Ethiopia and The Authors

SYNTHESIS OF NOVEL FLUFENAMIC ACID HYDRAZONES AS PREDICTED COX-2 INHIBITORS BY MOLECULAR MODELLING

Mashooq A. Bhat[1*], Mohamed A. Al-Omar[1], Ahmed H. Bakheit[1]

[1]Department of Pharmaceutical Chemistry, College of Pharmacy, King Saud University, Riyadh 11451, Saudi Arabia

(Received April 22, 2026; Revised September 28, 2026; Accepted September 30, 2026)

ABSTRACT. Flufenamic acid (FFA), *N*-(α,α,α-trifluoro-m-tolyl) anthranilic acid, is a derivative of *N*-phenyl anthranilic acid (fenamates). Flufenamic acid is a non-steroidal anti-inflammatory drug used as a potent analgesic and anti-inflammatory agent in the treatment of osteoarthritis, rheumatoid arthritis, and other painful musculoskeletal illnesses. In the present study, a novel series of hydrazone derivatives of flufenamic acid (**2**-**7**) were obtained by reacting different substituted aldehydes with flufenamic acid hydrazide. We prepared 2-[3-(trifluoromethyl) anilino] benzohydrazide (**1**) by esterifying flufenamic acid (**I**), followed by treatment with hydrazine hydrate (99%) in absolute ethanol. The structures of all synthesized compounds were confirmed by ^{1}H-NMR, ^{13}C-NMR, and LC/MS. Molecular docking against COX-1 (PDB ID: 3N8Y) and COX-2 (PDB ID: 5IKR) predicted that compounds **3** and **7** had the most favorable COX-2 binding energies in the series (-10.15 kcal mol^{-1}). These computational results indicate preferential binding within the applied docking model; however, they do not demonstrate biological potency or isoform selectivity. Compounds **3** and **7** are therefore proposed as candidates for subsequent enzymatic and cellular validation.

KEY WORDS: Flufenamic acid, Hydrazides, Hydrazones, COX-1/COX-2

INTRODUCTION

Nonsteroidal anti-inflammatory drugs (NSAIDs) remain a cornerstone in the management of pain, fever, and inflammation owing to their ability to inhibit cyclooxygenase (COX) enzymes involved in prostaglandin biosynthesis. The COX enzyme family comprises two major isoforms: COX-1, a constitutive enzyme responsible for physiological prostaglandin synthesis, which maintains gastric mucosal protection and renal function, and COX-2, an inducible isoform primarily expressed during inflammatory responses and pathological conditions, such as cancer and neurodegeneration. Conventional NSAIDs non-selectively inhibit both isoforms, often leading to gastrointestinal and renal side effects. Hence, the design of selective COX-2 inhibitors has gained significant importance to minimize adverse effects while preserving therapeutic efficacy.

Flufenamic acid (FFA), a member of the anthranilic acid (fenamate) class of NSAIDs, is well known for its potent anti-inflammatory, analgesic, and antipyretic activities mediated primarily through COX inhibition. Beyond its traditional NSAID profile, recent studies have revealed that FFA exerts multi-target pharmacological actions, including modulation of TRP ion channels, neuroprotective, anticonvulsant, and anticancer activities [1-2]. Flufenamic acid derivatives have also demonstrated inhibitory activity against 5-lipoxygenase (5-LOX) and inducible nitric oxide synthases (iNOS), thereby expanding their therapeutic scope to include oxidative stress and inflammatory disorders [3]. Moreover, structural modification of the FFA scaffold has yielded promising results in anticancer research, particularly through metal complexes and heterocyclic conjugates that exhibit sub-micromolar cytotoxic potency [4]. In the literature, N-arylhydrazone derivatives of mefenamic acid were synthesized and evaluated for analgesic and anti-

*Corresponding author. E-mail: mabhat@ksu.edu.sa
This work is licensed under the Creative Commons Attribution 4.0 International License

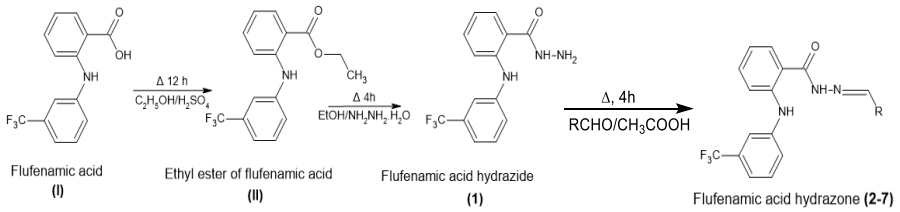
inflammatory activity. The results showed that replacing the acidic moiety of mefenamic acid with an N-arylhydrazone moiety can yield potent analgesic-anti-inflammatory compounds [5].

Molecular docking studies provide valuable insights into the binding orientation and affinity of designed ligands within the active site of target proteins, thereby assisting in the rational design of selective inhibitors [6]. The COX-2 enzyme possesses a hydrophobic channel and a secondary side pocket that differentiates it from COX-1, primarily due to a valine substitution at position 523 (Val 523) in place of isoleucine (Ile 523) in COX-1 [7]. This structural variation enlarges the COX-2 binding site, allowing bulky substituents to fit more effectively and facilitate selective inhibition. Key residues involved in ligand recognition and stabilization include Arg 120, Tyr 355, Ser 530, Tyr 385, and His 90, which contribute to hydrogen–bonding and π–π stacking interactions with the aromatic and heterocyclic moieties of inhibitors [8]. Flufenamic acid and its analogs typically anchor within the COX active site via hydrogen bonding to Arg 120 and Tyr 355, while the aromatic rings interact with the hydrophobic pocket composed of Val 349, Leu 352, and Phe 518. In this work, we used the X-ray crystal structure of human COX-2 to perform molecular docking and evaluate the binding affinities, hydrogen-bonding patterns, and hydrophobic interactions of the synthesized flufenamic acid hydrazone derivatives [9]. The docking outcomes were analyzed to predict the most favorable binding conformations and to rationalize the observed structure–activity relationship (SAR). These results provide a computational basis for understanding the molecular mechanism underlying COX-2 inhibition by the newly designed flufenamic acid hydrazones.

In continuation of our research, herein we report the synthesis and molecular docking studies of hydrazone derivatives of flufenamic acid [10-16]. The synthesized compounds were characterized by various spectroscopic methods and computationally evaluated for their binding affinity and interaction profiles with the COX-1/COX-2 enzyme active sites to rationalize structure–activity relationships and identify potential lead candidates for further pharmacological investigation.

RESULTS AND DISCUSSION

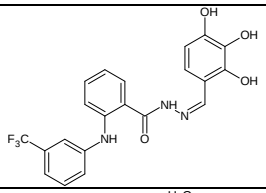
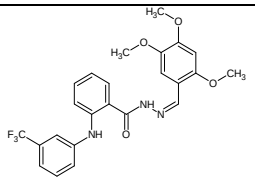
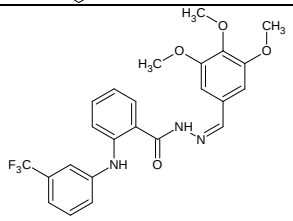
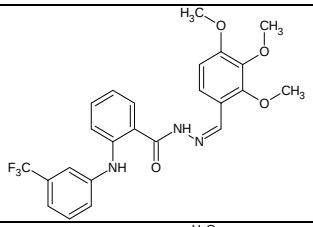
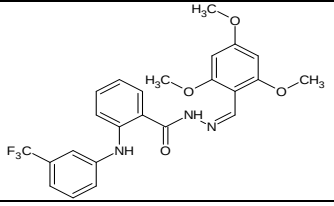
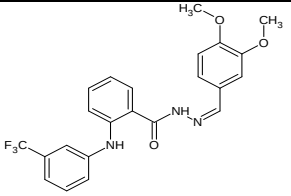
The target compounds (**1-7**) were synthesized following the designed synthetic protocol (Scheme 1).



Compd.	R
2	2, 3, 4-Trihydroxyphenyl
3	2, 3, 5-Trimethoxyphenyl
4	2, 3, 6-Trimethoxyphenyl
5	2, 4, 5-Trimethoxyphenyl
6	2, 3, 4-Trimethoxyphenyl
7	3, 4-Dimethoxyphenyl

Scheme 1. Synthetic route of compounds (**2-7**).

Table 1. Structures of the synthesized compounds (**2-7**).

Compd.	Structure	Compd.	Structure
2		**5**	
3		**6**	
4		**7**	

The structures of all synthesized compounds were confirmed by ^{1}H-NMR, ^{13}C-NMR, and mass spectrometric analysis, which were found to be in good agreement with the proposed structures. Compound **1** represents the key intermediate, and its ^{1}H-NMR spectrum exhibited characteristic singlets at δ 9.91 and 9.56 ppm corresponding to exchangeable NH protons. A broad signal at δ 4.59 ppm was assigned to an NH_2 group, indicating the presence of a primary amine functionality. The aromatic protons resonated as multiplets in the region δ 6.94–7.63 ppm. The ^{13}C-NMR spectrum further supported the structure, displaying signals for aromatic carbons along with a characteristic carbonyl carbon at δ 167.71 ppm. The mass spectrum showed a molecular ion peak at m/z 295 (M^+), consistent with the molecular formula. The formation of the final derivatives (**2-7**) was confirmed by the appearance of characteristic signals corresponding to the newly formed functionalities. In compound **2**, the presence of NH signals was evidenced by downfield singlets at δ 11.85 and 9.18 ppm. The singlet for N=CH appeared at δ 8.70 ppm, confirming the retention of the core scaffold. Aromatic protons appeared as multiplets between δ 6.98-7.81 ppm. A key diagnostic feature of the compounds is a singlet in the region δ 8.24–8.70 ppm, assigned to the azomethine (=CH) proton, confirming successful formation of the Schiff base linkage. Furthermore, all compounds in this series displayed two distinct singlets in the downfield region (δ ~11.5–11.8 and δ ~9.0–9.2 ppm), corresponding to amide NH protons, supporting the proposed structures. The aromatic region (δ 6.7–7.7 ppm) showed complex multiplet patterns consistent with substituted aromatic rings. The presence of methoxy substituents in the compounds was clearly indicated by singlets in the region δ 3.66–3.81 ppm. The integration of these signals confirmed the number of methoxy groups present in each compound. Substituent effects were evident from the chemical shift variations observed across the series. Electron-donating methoxy groups resulted in slight upfield shifts of aromatic protons, while the azomethine proton consistently appeared in the downfield region due to conjugation with the aromatic system. Overall, the spectral data clearly confirm the successful synthesis of the desired compounds. The disappearance of the primary amine signal (observed in **1**) and the concurrent appearance of the azomethine proton in compounds (**2-7**) provide strong evidence for

the progression of the condensation reaction. For the parent hydrazide **1**, the spectrum exhibited characteristic signals corresponding to aromatic carbons in the region δ 113–143 ppm, while the amide carbonyl carbon appeared as a distinct downfield resonance at δ ~167 ppm, confirming the presence of the –CONH– functionality. A characteristic quartet observed at δ ~129–130 ppm is attributed to the trifluoromethyl (–CF_3) carbon due to coupling with fluorine atoms, supporting the incorporation of the CF_3-substituted aniline moiety. In the hydrazone derivatives (**2-7**), the formation of the azomethine (–CH=N–) linkage was evidenced by the appearance of an imine carbon signal typically in the range δ ~158–165 ppm. Additionally, the amide carbonyl carbon consistently appeared in the downfield region (δ ~164–165 ppm), confirming retention of the hydrazide functionality after condensation. The aromatic carbon signals for all derivatives were distributed between δ ~104–145 ppm, reflecting the presence of multiple substituted phenyl rings. Compounds bearing electron-donating substituents such as a hydroxyl group in **2** and methoxy groups in (**3-7**) showed noticeable shifts in the aromatic region, particularly for substituted carbons attached to oxygen, which resonated at relatively deshielded positions (δ ~148–160 ppm). In methoxy-substituted derivatives (**3-7**), the –OCH_3 carbons appeared as distinct signals in the upfield region at δ ~55–63 ppm, confirming their presence. The variation in the number and position of methoxy groups across these derivatives was reflected in the corresponding number of aliphatic carbon signals and subtle changes in aromatic carbon chemical shifts. The combined spectroscopic data validate the proposed structures of all synthesized derivatives.

Docking studies

Cyclooxygenase enzymes, COX-1 and COX-2, are pivotal in mediating physiological processes related to inflammation and pain. The geometry and sequence identity of both cyclooxygenase isoforms (COX-1 and COX-2) are highly analogous. However, subtle differences, such as the presence of a Val 523 amino acid within the binding site of the COX-2 isozyme as opposed to an Ile 523 amino acid in the COX-1 isozyme, play a crucial role in drug selectivity. This minimal substitution induces significant alterations in the geometry and electron distribution of the COX-2 isoform, thereby unlocking a secondary binding pocket and exposing the polar amino acid Arg 513. Optimally occupying this newly unveiled secondary pocket and interacting with Arg 513 is hypothesized to enhance COX-2 selectivity. Investigating the interaction profiles of selected ligands within the binding pockets of ovine COX-1 (PDB ID: 3N8Y) and human COX-2 (PDB ID: 5IKR) structures supports comparison of predicted binding modes. Because the receptors are from different species and docking does not measure enzyme inhibition, the comparison is interpreted as hypothesis-generating rather than definitive evidence of biological selectivity. In this study, seven ligands (**1-7**) were subjected to docking studies to evaluate their binding affinities and selectivity towards COX-1 and COX-2 enzymes (Table 2, Table 3). Mefenamic acid was included as the reference ligand to contextualize the docking behavior of compounds (**1-7**). The reference produced docking energies of -6.99 kcal mol^{-1} against ovine COX-1 (PDB ID: 3N8Y) and -6.83 kcal mol^{-1} against human COX-2 (PDB ID: 5IKR) (Table 4). In the COX-1 complex, mefenamic acid formed hydrogen bonds with Tyr 385 and Ser 530, with donor-acceptor distances of 2.87 and 3.64 Å, respectively. Its binding pose was further stabilized by hydrophobic contacts with Val 116, Val 349, Tyr 355, Leu 384, Tyr 385, Trp 387, Ile 523, Ala 527, and Leu 531. In the COX-2 complex, hydrogen bonds were observed with Tyr 385 and Ser 530 at donor-acceptor distances of 2.82 and 2.77 Å, respectively, together with hydrophobic contacts involving Val 349, Leu 352, Tyr 385, Trp 387, Val 523, Ala 527, and Leu 531. The recurrence of Tyr 385 and Ser 530, together with residues lining the hydrophobic channel, supports placement of mefenamic acid within the cyclooxygenase binding region in both receptor structures. The small energy difference between COX-1 and COX-2 (0.16 kcal mol^{-1}) suggests similar predicted docking affinity under the applied protocol; therefore, these docking data should be used as a reference for pose and score comparison rather than as evidence of isoform selectivity. Because the comparison

uses ovine COX-1 and human COX-2 structures, cross-isoform interpretation should also account for the mixed-species receptor set.

Table 2. Hydrogen bond interactions between ligands and COX-1 (PDB ID: 3N8Y).

Ligand	Receptor	Donor Type	Acceptor Type	DIST H-A	DIST D-A	DON_ANGLE	Scoring
1	OH Tyr (A)385	O3	N3	2.01	2.97	175.42	-8.37
	OG Ser (A) 530	O3	O2	1.91	2.84	163.01	
	OG Ser (A) 530	N3	O3	2.21	3.1	143.65	
2	OH Tyr (A)348	O3	O2	3.25	3.76	115.28	-7.49
	OH Tyr (A)385	O3	O2	2.12	2.97	147.39	
	OG Ser (A) 530	O3	Nam	2.4	3.27	150.69	
	OG Ser (A) 530	Nam	O3	2.45	3.27	136.17	
3	OH Tyr (A)385	O3	Nam	2.34	3.27	162.87	-5.31
	OG Ser (A) 530	O3	O2	1.87	2.81	169.35	
	CA Gly (A)533	Nam	O2	3.05	3.45	104.83	
4	OH Tyr (A)348	O3	O2	3.26	3.78	115.49	-6.27
	OH Tyr (A)385	O3	O2	2.58	3.33	135.74	
	OG Ser (A) 530	O3	Nam	2.75	3.61	149.58	
	OG Ser (A) 530	Nam	O3	2.76	3.61	140.24	
5	OH Tyr (A)385	O3	N2	1.59	2.49	154.4	-6.40
	OG Ser (A) 530	O3	Nam	2.82	3.3	111.64	
	NamGly(A)533	Nam	O2	3.21	3.58	103.18	
6	OH Tyr (A)385	O3	N2	1.72	2.56	144.33	-5.55
	OG Ser (A) 530	O3	Nam	2.92	3.52	121.74	
	OG Ser (A) 530	Nam	O3	3.13	3.52	104.11	
7	OH Tyr (A)348	O3	O2	3.4	4.03	125.18	-6.16
	OG Ser (A) 530	Nam	O3	2.62	3.01	101.88	
	OG Ser (A) 530	O3	N2	1.86	2.78	159.35	

Table 3. Hydrogen bond interactions between ligands and COX-2 (PDB ID: 5IKR).

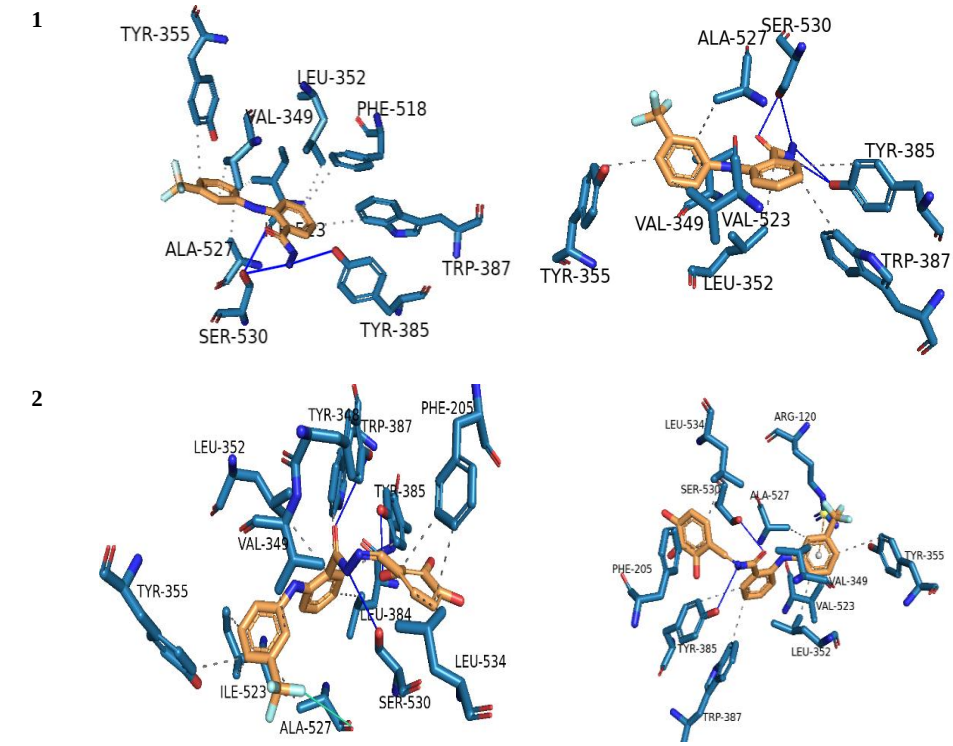
Ligands	Receptor	Donor Type	Acceptor type	DIST H-A	DIST D-A	DOND ANGLE	Scoring
1	Tyr (A) 385	O3	N3	2.31	3.16	148.16	-8.01
	Tyr (A) 385	Nam	O3	2.19	2.99	133.64	
	Ser (A) 530	N3	O3	2.08	2.99	146.4	
	Ser (A) 530	O3	O2	1.89	2.76	149.16	
2	Tyr (A) 385	O3	Nam	2.45	3.37	160.82	-9.88
	Ser (A) 530	O3	O2	1.91	2.85	163.83	
3	Tyr (A) 385	Nam	N3	1.71	2.66	165.06	-10.15
	Ser (A) 530	Nam	N3	2.05	2.66	119.63	
4	Asn (A) 410	O3	O2	2.84	3.31	109.03	-8.50
	Glu (A) 416	O3	N2	1.84	2.59	140.41	
5	Tyr (A) 385	O3	O2	1.6	2.55	166.27	-9.66
	Ser (A) 530	O3	N2	1.66	2.59	161.96	
6	Tyr (A) 385	O3	Npl	3.01	3.76	135.3	-9.01
	Ser (A) 530	O3	O2	1.84	2.71	148.88	
	Leu (A) 531	Nam	N2	3.6	4.09	112.33	
7	Tyr (A) 348	O3	O2	3.25	3.7	110.22	-10.15
	Tyr (A) 385	O3	Nam	3.03	3.88	148.72	
	Tyr (A) 385	Nam	O3	2.94	3.88	153.59	
	Ser (A) 530	O3	N2	1.83	2.7	148.58	

The docking analysis reported hydrogen-bond contacts in Tables 2 and 3. Additional nonpolar contacts are visible in the interaction diagrams in Figure 1, but compound-specific hydrophobic contacts were not available in a validated tabular output; therefore, unsupported residue assignments were not used to infer selectivity.

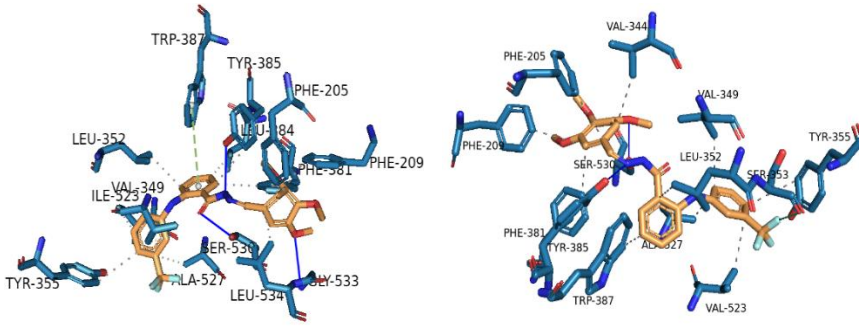
Table 4. Docking energies and binding-site interactions of mefenamic acid with COX-1 and COX-2.

Target (PDB ID)	Docking energy (kcal mol^{-1})	Hydrogen bonds (D-A distance, Å)	Hydrophobic contacts
Ovine COX-1 (3N8Y)	-6.99	Tyr 385 (2.87); Ser 530 (3.64)	Val 116, Val 349, Tyr 355, Leu 384, Tyr 385, Trp 387, Ile 523, Ala 527, Leu 531
Human COX-2 (5IKR)	-6.83	Tyr 385 (2.82); Ser 530 (2.77)	Val 349, Leu 352, Tyr 385, Trp 387, Val 523, Ala 527, Leu 531

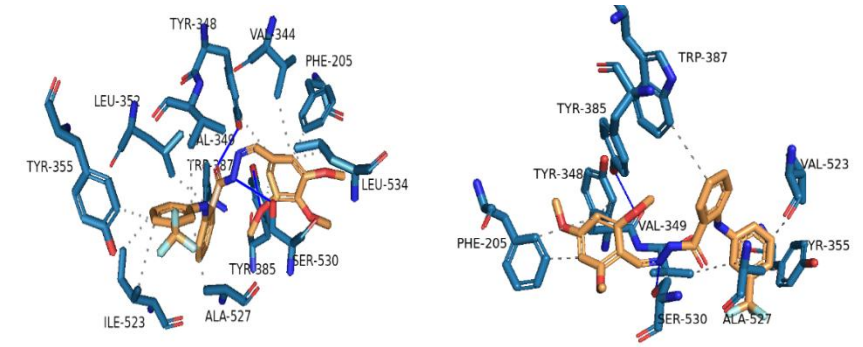
Interpretive note: Docking scores are computational estimates and should not be interpreted as experimental inhibition constants.



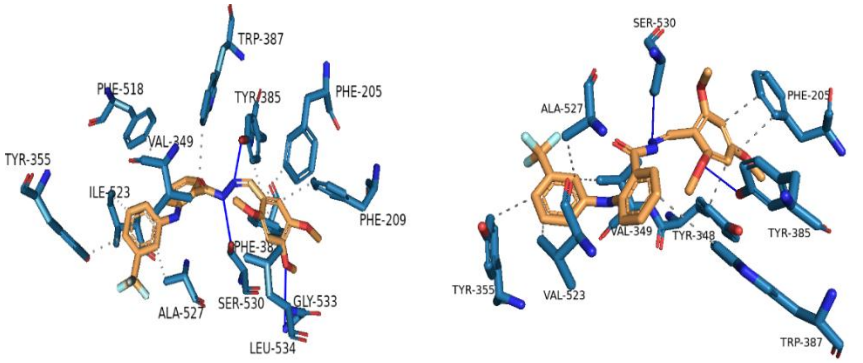
3


TRP-387
TYR-385
PHE-205
LEU-352
PHE-209
VAL-349
ILE-523
SER-530
TYR-355
ALA-527
LEU-534
GLY-533
VAL-344
PHE-205
VAL-349
TYR-355
SER-530
LEU-352
PHE-381
TYR-385
TRP-387
VAL-523

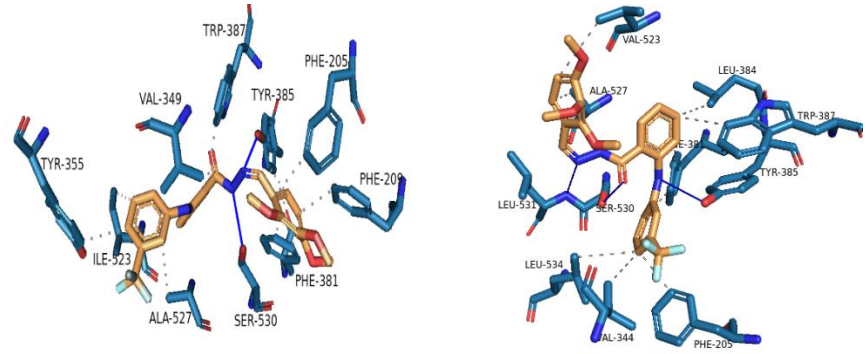
4


TYR-348
VAL-344
PHE-205
LEU-352
VAL-349
TYR-355
LEU-534
TYR-385
SER-530
ILE-523
ALA-527
TRP-387
TYR-385
TYR-348
VAL-523
VAL-349
PHE-205
TYR-355
SER-530
ALA-527

5


TRP-387
PHE-518
TYR-385
PHE-205
VAL-349
TYR-355
ILE-523
PHE-209
PHE-381
ALA-527
SER-530
GLY-533
LEU-534
SER-530
ALA-527
PHE-205
VAL-349
TYR-348
TYR-385
TYR-355
VAL-523
TRP-387

6


TRP-387
PHE-205
VAL-349
TYR-385
TYR-355
PHE-209
ILE-523
PHE-381
ALA-527
SER-530
VAL-523
LEU-384
ALA-527
TRP-387
TYR-385
LEU-531
SER-530
LEU-534
VAL-344
PHE-205

7

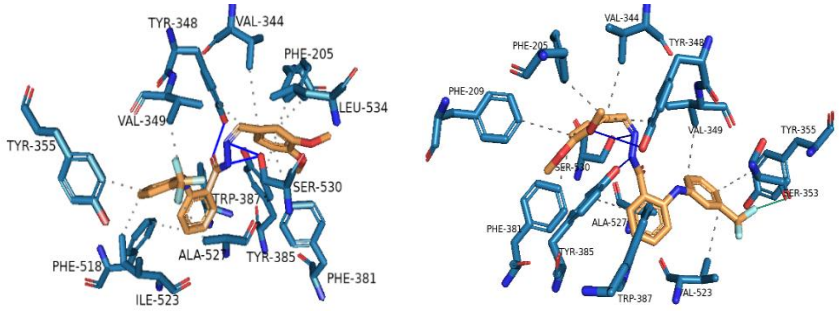


Figure 1. Molecular docking interactions of (**1-7**) with COX-1 and COX-2.

COX-1 (PDB ID: 3N8Y): The ligands formed predicted hydrogen-bond contacts with residues including Tyr 385, Ser 530, Tyr 348, and Gly 533, depending on the compound (Table 2). These contacts may contribute to pose stabilization, but their presence alone does not establish inhibitory potency.

COX-2 (PDB ID: 5IKR): Predicted hydrogen-bond contacts were observed principally with Tyr 385 and Ser 530, with additional contacts for selected ligands (Table 3). The docking poses suggest plausible binding within the cyclooxygenase channel; nevertheless, experimental enzyme assays are required to establish inhibition and isoform selectivity.

Nonpolar contacts and interpretation

COX-1: The interaction diagrams suggest nonpolar contacts within the COX-1 channel. Because compound-residue hydrophobic contacts were not exported in a validated, systematic dataset, no compound-specific contact list is claimed here.

COX-2: The COX-2 binding channel contains structural features that may accommodate the ligands, including the region surrounding Val 523. However, the present docking output does not substantiate specific Val 523 contacts for compounds 3 or 7; these assignments were therefore removed.

Selectivity and potency of compounds

Among the seven docked ligands, compounds **3** and **7** produced the most favourable predicted COX-2 binding energies (-10.15 kcal mol^{-1}), compared with -5.31 and -6.16 kcal mol^{-1}, respectively, for COX-1 in the applied protocol. This numerical difference indicates a preference within the docking model rather than experimentally proven potency or selectivity. For compound **3**, Table 3 reports predicted hydrogen-bond contacts with Tyr 385 and Ser 530; no Arg 513 hydrogen bond is present in the tabulated output. Compound **7** showed predicted contacts with Tyr 348, Tyr 385, and Ser 530. The docking results identify compounds **3** and **7** as candidates for follow-up COX-1/COX-2 enzyme inhibition assays, selectivity-index determination, and cellular anti-inflammatory studies.

EXPERIMENTAL

Flufenamic acid, containing an acidic group, was converted to its ethyl ester by reacting with absolute ethanol in the presence of a catalytic amount of concentrated sulfuric acid. The ethyl

ester of flufenamic acid reacted with 99% hydrazine hydrate in the presence of absolute alcohol to obtain the hydrazide derivative. In the final step, flufenamic hydrazide was reacted with various substituted benzaldehydes to form flufenamic acid hydrazones. The purity of the compounds was confirmed by thin-layer chromatography (TLC). The compounds were confirmed by their melting point, ^{1}H-NMR, ^{13}C-NMR, LC/MS, and elemental analysis.

*Synthesis of ethyl 2-[3-(trifluoromethyl)anilino] benzoate (**II**)*

A solution of flufenamic acid (**I**) (10 mmol), absolute ethanol (10 mL), and concentrated sulfuric acid (1 mL) was heated under reflux for 12 h. The solvent was evaporated under reduced pressure; the remaining contents were cooled to room temperature, neutralized with a concentrated solution of sodium bicarbonate, and then the aqueous solution was extracted with ethyl acetate (3 times × 20 mL). The combined ethyl acetate extracts were dried, and the solvent was removed under reduced pressure to yield the corresponding ester (**II**) in 80-85% yield.

*Synthesis of 2-[3-(trifluoromethyl) anilino] benzohydrazide (**1**)*

A solution of hydrazine hydrate (99.9%, 5 mmol) and ethyl ester of flufenamic acid (**II**) (1 mmol) was brought to gentle reflux for the appropriate 4 h, then cooled to room temperature. The solid formed was filtered, washed with several portions of water, and dried by suction. Crystallization from EtOH afforded the corresponding flufenamic acid hydrazide (**1**). Yield: 80 %; mp: 136-138 °C (reported: 134-136 °C); ^{1}H-NMR (500 MHz, DMSO-d_6) δ: 9.91 (s, D_2O exch., 1H, NH); 9.56 (s, D_2O exch.,1H, NH), 7.62-7.63 (m, 1H, ArH), 7.29-7.47 (m, 5H, ArH), 6.94-7.21 (m, 2H, ArH), 4.59 (br. s, D_2O exch., 2H, NH_2); ^{13}C-NMR δ: 113.80, 116.72, 116.91, 119.93, 120.84, 121.29, 123.01, 125.18, 128.58, 129.80-130.55 (m, -CF3), 131.55, 142.15, 143.10, 167.71. MS m/z (%): 295 (M^+) [8].

*Synthesis of 2-[3-(trifluoromethyl) anilino]-N'-[(Z)-(substituted phenyl) methylidene] benzohydrazide (**2-7**)*

A solution of flufenamic hydrazide (**1**) (1 g, 0.004 mol) in absolute ethanol (10 mL) was reacted for 4 h with different types of substituted benzaldehydes in the presence of glacial acetic acid to form flufenamic acid hydrazones. The solid obtained was purified by crystallization from EtOH, filtered, and dried to give the desired compound [9].

*2-[3-(trifluoromethyl) anilino]-N'-[(Z)-(2,3,4-trihydroxyphenyl) methylidene] benzohydrazide (**2**).* Yield: 80%; mp: 230-232 °C; ^{1}H-NMR (500 MHz, DMSO-d_6) δ: 11.85 (s, D_2O exch., 1H, NH), 9.18 (s, D_2O exch., 1H, NH), 8.70 (s, 1H, =CH), 7.81 (dd, *J* = 7.8, 1.8 Hz, 1H, Ar-H), 7.72 (s, 1H, Ar-H), 7.47 – 7.29 (m, 4H), 7.16 (d, *J* = 7.7 Hz, 1H, Ar-H), 7.07 (d, *J* = 8.4 Hz, 1H, Ar-H), 6.98 (td, *J* = 7.4, 4.7 Hz, 2H, Ar-H); ^{13}C-NMR (125 MHz, DMSO-d_6) δ: 56.2, 112.3, 114.4, 117.4, 118.0, 120.7, 121.2, 121.8, 122.0, 122.7, 125.9, 129.8, 130.9, 132.1, 132.6, 142.8, 143.8, 143.9, 158.3, 165.0; MS m/z (%): 431.00 [M^+]; $C_{21}H_{16}F_3N_3O_4$; 431.36; C (58.47%) H (3.74%) N (9.74%).

*2-[3-(trifluoromethyl) anilino]-N'-[(Z)-(3,4,5-trimethoxyphenyl) methylidene] benzohydrazide (**3**).* Yield: 78%; mp: 240-242 °C; ^{1}H-NMR (500 MHz, DMSO-d_6) δ: 11.88 (s, D_2O exch., 1H, NH), 9.08 (s, D_2O exch., 1H, NH), 8.24 (s, 1H, =CH), 7.64 (d, *J* = 7.7 Hz, 1H, Ar-H), 7.42 (s, 2H, Ar-H), 7.37 (s, 3H, Ar-H), 7.20 – 7.13 (m, 1H, Ar-H), 7.01 (s, 1H, Ar-H), 6.97 (s, 2H, Ar-H), 3.79 (s, 6H, 2×OCH_3), 3.66 (d, *J* = 1.0 Hz, 3H, OCH_3); ^{13}C-NMR (125 MHz, DMSO-d_6) δ: 56.4, 60.6, 104.7, 114.3, 117.3, 118.2, 120.9, 121.6, 122.5, 125.0, 129.8, 130.3, 130.9, 132.6, 139.7, 142.6,

143.9, 148.2, 153.7, 165.0; MS m/z (%): 473.00 [M^+]; $C_{24}H_{22}F_3N_3O_4$; 473.44; C (60.89%) H (4.68%) N (8.88%).

*2-[3-(trifluoromethyl) anilino]-N'-[(Z)-(2,4,6-trimethoxyphenyl) methylidene] benzohydrazide (**4**).* Yield: 75%; mp: 250-252 °C; ^{1}H-NMR (500 MHz, DMSO-d_6) δ: 11.51 (s, D_2O exch., 1H, NH), 9.20 (s, D_2O exch., 1H, NH), 8.49 (s, 1H, =CH), 7.65 (d, *J* = 7.4 Hz, 1H, Ar-H), 7.38 (d, *J* = 7.6 Hz, 3H, Ar-H), 7.34 (d, *J* = 8.4 Hz, 1H, Ar-H), 7.16 (d, *J* = 7.6 Hz, 1H, Ar-H), 6.97 (s, 1H, Ar-H), 6.24 (s, 3H, Ar-H), 3.77 (d, *J* = 17.2 Hz, 9H, 3×OCH_3); ^{13}C-NMR (125 MHz, DMSO-d_6) δ: 55.9, 56.4, 91.6, 104.4, 114.3, 117.3, 117.8, 120.7, 121.7, 122.4, 129.7, 130.7, 130.9, 132.3, 142.7, 143.9, 144.6, 160.5, 162.8, 164.6; MS m/z (%): 473.00 [M^+]; $C_{24}H_{22}F_3N_3O_4$; 473.44; C (60.89%) H (4.68%) N (8.88%).

*2-[3-(trifluoromethyl) anilino]-N'-[(Z)-(2,4,5-trimethoxyphenyl) methylidene] benzohydrazide (**5**).* Yield: 70%; mp: 248-250 °C; ^{1}H-NMR (500 MHz, DMSO-d_6) δ: 11.73 (s, D_2O exch., 1H, NH), 9.20 (s, D_2O exch., 1H, NH), 8.62 (s, 1H, =CH), 7.66 (dd, *J* = 7.8, 1.6 Hz, 1H, Ar-H), 7.39 – 7.34 (m, 4H, Ar-H), 7.30 (d, *J* = 2.0 Hz, 1H, Ar-H), 7.16 (d, *J* = 7.7 Hz, 1H, Ar-H), 7.07 (s, 1H, Ar-H), 7.01 – 6.95 (m, 1H, Ar-H), 6.71 (s, 1H, Ar-H), 3.81 (s, 6H, 2×OCH_3), 3.70 (s, 3H, OCH_3); ^{13}C-NMR (125 MHz, DMSO-d_6) δ: 56.3, 57.0, 98.3, 107.9, 114.3, 117.3, 120.7, 121.7, 122.1, 123.6, 125.8, 129.7, 130.9, 132.5, 141.0, 142.7, 144.0, 152.6, 153.9, 155.2, 156.0, 159.6, 164.8; MS m/z (%): 473.00 [M^+]; $C_{24}H_{22}F_3N_3O_4$; 473.44; C (60.89%) H (4.68%) N (8.88%).

*2-[3-(trifluoromethyl) anilino]-N'-[(Z)-(2,3,4-trimethoxyphenyl) methylidene] benzohydrazide (**6**).* Yield: 78%; mp: 260-262 °C; ^{1}H-NMR (500 MHz, DMSO-d_6) δ: 11.80 (s, D_2O exch., 1H, NH), 9.19 (s, D_2O exch., 1H, NH), 8.52 (s, 1H, =CH), 7.74 – 7.63 (m, 1H, Ar-H), 7.57 (d, *J* = 8.9 Hz, 1H, Ar-H), 7.46 – 7.31 (m, 5H, Ar-H), 7.16 (d, *J* = 7.6 Hz, 1H, Ar-H), 6.99 (t, *J* = 7.4 Hz, 1H, Ar-H), 6.90 (d, *J* = 8.9 Hz, 1H, Ar-H), 3.80 (d, *J* = 9.1 Hz, 6H, 2×OCH_3), 3.73 (s, 3H, OCH_3); ^{13}C-NMR (125 MHz, DMSO-d_6) δ: 56.5, 61.0, 63.3, 109.3, 114.3, 118.0, 120.8, 121.0, 121.7, 129.7, 130.9, 134.0, 142.0, 143.8, 144.0, 153.2, 165.0; MS m/z (%): 473.00 [M^+]; $C_{24}H_{22}F_3N_3O_4$; 473.44; C (60.89%) H (4.68%) N (8.88%).

*2-[3-(trifluoromethyl) anilino]-N'-[(Z)-(3,4-dimethoxyphenyl) methylidene] benzohydrazide (**7**)* Yield: 78%; mp: 255-257 °C; ^{1}H-NMR (500 MHz, DMSO-d_6) δ 11.77 (s, D_2O exch., 1H, NH), 9.11 (s, D_2O exch., 1H, NH), 8.25 (s, 1H, =CH), 7.64 (d, *J* = 7.8 Hz, 1H, Ar-H), 7.38 (dt, *J* = 27.5, 7.9 Hz, 5H), 7.32 – 7.26 (m, 1H), 7.24 – 7.07 (m, 2H), 7.06 – 6.88 (m, 2H), 3.76 (d, *J* = 2.1 Hz, 6H).; MS m/z (%): 443.00 [M+]; $C_{23}H_{20}F_3N_3O_3$; 443.41; C (62.30%) H (4.55%) N (9.48%).

Molecular docking methodology

Molecular docking studies were performed to determine the optimal binding poses of docked ligands within the receptor's active site. This facilitated interpreting the reported biological activities by analyzing ligand-receptor interaction patterns. The docking process followed a standardized workflow encompassing ligand preparation, receptor preparation, grid generation, validation of the docking protocol, and the docking studies.

Ligand preparation

The ligands studied were nonsteroidal anti-inflammatory drugs (NSAIDs), including parent and substituted flufenamic hydrazones. The 2D structures of these compounds were created using Marvin Sketch (https://chemaxon.com/marvin) and saved in sdf format [17]. These files were imported into Avogadro2, where geometry optimization was carried out using the Generalized Amber Force Field (GAFF), owing to its compatibility with Avogadro [18-19]. The optimized

ligands were subsequently saved in pdbqt format. Docking simulations were performed using AutoDock (The Scripps Research Institute), a widely used tool that predicts binding affinities and inhibition constants, providing insights relevant to in vitro analyses. All ligands were prepared, and torsion angles were adjusted using AutoDock's ligand preparation tools [20].

Receptor preparation

Receptor structures were obtained in PDB format and prepared using AutoDockTools. Water molecules were removed, nonpolar hydrogens were added, charges were assigned, and grid-box parameters were defined around the co-crystallized ligand-binding sites. COX-1 and COX-2 were represented by PDB IDs 3N8Y (ovine COX-1) and 5IKR (human COX-2), respectively. Mefenamic acid was intended as a reference compound; however, its numerical docking output was present in the available dataset and is therefore reported or used for comparative conclusions. Binding energies are reported in kcal mol^{-1} using the negative sign convention, where a more negative value denotes a more favorable predicted docking score. Best-ranked poses were examined using PLIP and visualized using PyMOL (version 3.1.1) [21-22].

Validation of docking protocol

The docking protocol was validated by re-docking the co-crystallized ligands into the corresponding binding sites of COX-1 (PDB ID: 3N8Y) and COX-2 (PDB ID: 5IKR) (Fig. 2). The predicted re-docked poses were superimposed on the experimentally determined ligand conformations, and the root-mean-square deviation (RMSD) was calculated to assess the ability of the docking protocol to reproduce the crystallographic binding orientations. The obtained RMSD values were 0.312 Å for COX-1 (3N8Y) and 0.283 Å for COX-2 (5IKR), as illustrated in Figures A and B, respectively. Both values were substantially below the predefined acceptance threshold of 2.0 Å, demonstrating close agreement between the re-docked and crystallographic ligand poses and supporting the reliability of the docking protocol for predicting ligand-binding conformations within the investigated COX-1 and COX-2 binding sites.

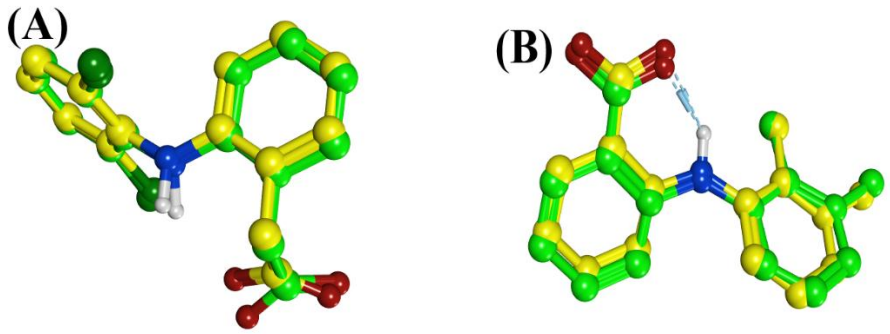


Figure 2. Overlay of the crystallographic and re-docked ligand poses used to validate the docking protocol for (A) COX-1 (PDB ID: 3N8Y; RMSD = 0.312 Å) and (B) COX-2 (PDB ID: 5IKR; RMSD = 0.283 Å). The low RMSD values confirm close agreement between the predicted and experimentally determined binding poses.

CONCLUSION

The synthetic route used to synthesize the target compounds is described in the synthetic route shown in Scheme 1. Ethyl 2-[3-(trifluoromethyl)anilino] benzoate (**II**) was prepared according to the method reported in the literature, using flufenamic acid (**I**) as a starting material. The 2-[3-(trifluoromethyl) anilino] benzohydrazide (**1**) was prepared by esterification of flufenamic acid, followed by treatment with hydrazine hydrate (99%) in absolute ethanol. Flufenamic acid hydrazide was reacted with various phenyl-substituted aldehydes to form the hydrazones (**2-7**). The synthesized compounds were confirmed using spectral data such as ^{1}H-NMR, ^{13}C-NMR, and LC/MS. Docking against COX-1 and COX-2 predicted that compounds 3 and 7 had the most favorable COX-2 binding energies in the investigated series. These findings support their prioritization for follow-up studies but do not prove COX-2 inhibition, potency, or isoform selectivity. Experimental COX-1/COX-2 enzyme assays, calculation of selectivity indices, and appropriate cellular studies are required to validate the computational predictions.

ACKNOWLEDGMENT

The authors acknowledge and appreciate the Ongoing Research Funding Program (ORF-2026-740), King Saud University, Riyadh, Saudi Arabia.

Data availability

The data used to support the findings of this study are available from the corresponding author upon request. Samples of the compounds (**1-7**) in pure form are available from the authors.

Conflicts of interest

The authors declare that they have no known competing financial interests or personal relationships that could have appeared to influence the work reported in this paper.

Funding

This research was supported by the Ongoing Research Funding Program (ORF-2026-740) at King Saud University in Riyadh, Saudi Arabia.

REFERENCES

1. Chen, J.; Chang, Y.; Zhu, J.; Peng, Y.; Li, Z.; Zhang, K.; Zhang, Y.; Lin, C.; Lin, Z.; Pan, S.; Huang, K. Flufenamic acid improves survival and neurologic outcome after successful cardiopulmonary resuscitation in mice. *J. Neuroinflammation* **2022**, 19, 214.
2. Salmanzadeh, H.; Halliwell, R.F. Antiseizure properties of fenamate NSAIDs determined in mature human stem-cell derived neuroglial circuits. *Front. Pharmacol.* **2024**, 15, 1385523.
3. Hussein, S.; Fayed, E.A.; Ragab, A.; Abusaif, M.S.; Ammar, Y.A.; El-Sayed Mansou, R.; Musa, A.; Ramsis, T.M. Flufenamic acid-based sulfonohydrazide and acetamide derivatives NSAI as inhibitors of multi-targets COX-1/COX-2/5-LOX: Design, synthesis, in silico ADMET and binding mode studies. *BMC Chem.* **2025**, 19, 271.
4. Li, Y.; Fang, J.; Singh, K.; Ortu, F.; Suntharalingam, K. An immunogenic anti-cancer stem cell bi-nuclear copper (II)-flufenamic acid complex. *Dalton trans.* **2024**, 53, 6410-6415.
5. Almasirad, A.; Tajik, M.; Bakhtiari, D.; Shafiee, A.; Abdollahi, M.; Zamani, M.J.; Khorasani, R.; Esmaily, H. Synthesis and analgesic activity of N-Arylhydrazone derivatives of mefenamic acid. *J. Pharm. Pharm. Sci.* **2005**, 8, 419-25.

6. Azam, F. Identifying a novel class of lead compounds for monoacylglycerol lipase inhibition: an integrated computational study. *Cell Mol. Biol.* **2025**, 71, 103-111.
7. Blobaum, A.L.; Marnett, L.J. Structural and functional basis of cyclooxygenase inhibition. *J. Med. Chem.* **2007**, 50, 1425-1441.
8. Vecchio, A.J.; Orlando, B.J.; Nandagiri, R.; Malkowski, M.G. Investigating substrate promiscuity in cyclooxygenase-2: the role of Arg-120 and residues lining the hydrophobic groove. *J. Biol. Chem.* **2012**, 287, 24619-30.
9. Hussein, S.; Fayed, E.A.; Ragab, A.; Abusaif, M.S.; Ammar, Y.A.; El-Sayed Mansou, R.; Musa, A.; Ramsis, T. M. Flufenamic acid-based sulfonohydrazide and acetamide derivatives NSAI as inhibitors of multi-targets COX-1/COX-2/5-LOX: design, synthesis, in silico ADMET and binding mode studies. *BMC Chem.* **2025**, 19, 271.
10. Bhat, M.A.; Al-Omar, M.A.; Alsaif, N.A.; Almehizia, A.A.; Naglah, A.M.; Razak, S.; Khan, A.A.; Ashraf, N.M. Novel sulindac derivatives: synthesis, characterisation, evaluation of antioxidant, analgesic, anti-inflammatory, ulcerogenic and COX-2 inhibition activity. *J. Enzyme Inhib. Med. Chem.* **2020**, 35, 921-934.
11. Bhat, M.A.; Al-Omar, M.A.; Raish, M.; Ansari, M.A.; Abuelizz, H.A.; Bakheit, A.H.; Naglah, A. M. Indole derivatives as cyclooxygenase inhibitors: Synthesis, biological evaluation and docking studies. *Molecules* **2018**, 23, 250.
12. Bhat, M.A.; Al-Omar, M.A.; Ansari, M.A.; Zoheir, K.M.; Imam, F.; Attia, S.M.; Bakheet, S. A.; Nadeem, A.; Korashy, H.M.; Voronkov, A.; Berishvili, V.; Ahmad, S.F. Design and synthesis of N-arylphthalimides as inhibitors of glucocorticoid-induced TNF receptor-related protein, proinflammatory mediators, and cytokines in carrageenan-induced lung inflammation. *J. Med. Chem.* **2015**, 58, 8850-8867.
13. Bhat, M.A.; Tüzün, B.; Koyuncu, I.; Temiz, E.; Taslimi, P.; Naglah, A.M.; Al-Omar, M.A.; Džudžević-Čančar, H. Synthesis, molecular modelling and choline esterase enzyme inhibitory activity of novel enaminone derivatives of sulfonamides. *Bull. Chem. Soc. Ethiop.* **2024**, 38, 1351-1368.
14. Almehizia, A.A., Al-Omar, M.A., Naglah, A.M., Bhat, M.A. Metal-urea complexes as primary precursors to generate VO_2, ZrO_2, NbO_2, TaO_2, Ga_2O_3 and TeO_2 oxides in the nanoscale range by thermal decomposition route. *Bull. Chem. Soc. Ethiop.* **2024**, 38, 1003-1012.
15. Aboul-Fadl, T.; Abdel-Aziz, H.A.; Kadi, A.; Bari, A.; Ahmad, P.; Al-Samani, T.; Ng, S.W. Microwave-assisted one-step synthesis of fenamic acid hydrazides from the corresponding acids. *Molecules* **2011**, 16, 3544-3551.
16. Bhat, M.A.; Naglah, A.M.; Bakheit, A.H.; Al-Omar, M.A. Synthesis, characterization, and molecular modelling of novel 1,3,4-oxadiazole derivatives of mefenamic acid. *Polish J. Chem. Tech.* **2024**, 26, 102-112.
17. ChemAxon. MarvinSketch. Available online: https://chemaxon.com/marvin (accessed on 18 March 2022).
18. Hanwell, M.D.; Curtis, D.; Lonie, D.C.; Vandermeersch, T.; Zurek, E.; Hutchison, G.R. Avogadro: An advanced semantic chemical editor, visualization, and analysis platform. *J. Cheminform.* **2012,** 4, 17.
19. Wang, J.; Wolf, R.M.; Caldwell, J.W.; Kollman, P.A.; Case, D.A. Development and testing of a general amber force field. *J. Comput. Chem.* **2004**, 25, 1157-1174.
20. Adasme, M.F.; Linnemann, K.L.; Bolz, S.N.; Kaiser, F.; Salentin, S.; Haupt, V.J.; Schroeder, M. PLIP 2021: Expanding the scope of the protein–ligand interaction profiler to DNA and RNA. *Nucleic Acids Res.* **2021**, 49, W530-W534.
21. Castro-Alvarez, A.; Costa, A. M.; Vilarrasa, J. The performance of several docking programs at reproducing protein–macrolide-like crystal structures. *Molecules* **2017**, 22, 136.
22. Pagadala, N.S.; Syed, K.; Tuszynski, J. Software for molecular docking: A review. *Biophys Rev*. **2017**, 9, 91-102.